



Effect of water and rock composition on re-strengthening of cohesive faults during the deceleration phase of seismic slip pulses

M. Violay^{a,*}, F. Passelegue^a, E. Spagnuolo^b, G. Di Toro^{b,c}, C. Cornelio^a

^a Laboratory of Experimental Rock Mechanics EPFL, Lausanne, Switzerland

^b Istituto Nazionale di Geofisica e Vulcanologia, Rome, Italy

^c Dipartimento di Geoscienze, Università degli studi di Padova, Padua, Italy

ARTICLE INFO

Article history:

Received 6 June 2018

Received in revised form 26 April 2019

Accepted 22 June 2019

Available online 3 July 2019

Editor: J.-P. Avouac

Keywords:

earthquake

friction

re-strengthening

ground motions

water effect

ABSTRACT

The elastic strain energy release rate and seismic waves emitted during earthquakes are controlled by the on-fault temporal evolution of the shear stress during rupture propagation. High velocity friction experiments highlighted that shear stress on the fault surface evolves rapidly during seismic slip pulses. This temporal evolution of shear stress is controlled by both fault weakening at seismic slip initiation and re-strengthening rate towards the end of slip. While numerous studies focused on fault weakening, less attention was given to co-seismic re-strengthening processes. Here we performed 53 friction experiments (normal stress ≤ 30 MPa, slip-rate ≤ 6.5 m s⁻¹) imposing constant slip acceleration and deceleration (7.8 m s⁻²), on cohesive Carrara marble (99% calcite) and micro-gabbro (silicate-built rock) under dry, vacuum and water pressurized conditions. Microstructural observations showed that micro-gabbro accommodated seismic slip by bulk melting of the sliding surfaces, whereas Carrara marble by coupled decarbonation and grain-size dependent crystal plastic processes. Under room humidity conditions and low imposed power density (i.e., product of normal stress per slip rate), re-strengthening rate during the deceleration stage was up to ~ 17 times faster in marble than in microgabbro. In the latter, the re-strengthening rate increased slightly with the power density. The presence of water enhanced further this trend. On the contrary, in marbles the re-strengthening rate decreased drastically with power density and in the presence of water. Our experimental observations highlighted the first order importance of the mineralogy and rheology of the slip zone materials and, to a second order, of the presence of water in controlling co-seismic re-strengthening of faults during seismic slip deceleration.

© 2019 Elsevier B.V. All rights reserved.

1. Introduction

Earthquakes are the result of sudden slip along faults, which releases the elastic strain and gravitational energy stored in the wall rocks (Reid, 1910; Kanamori and Rivera, 2013). Damage associated with earthquakes is due to the radiation of elastic waves during seismic rupture propagation (Stein and Wysession, 2009; Madariaga and Olsen, 2002; Marty et al., 2019) and to dynamic stress concentration at the rupture front (e.g., Andrews, 2005). The intensity and the frequency of seismic waves (ground motions) are controlled by the rupture length and by the abrupt variations in rupture and slip velocities along fault during earthquakes (Brune, 1970; Madariaga, 1976). Seismic rupture (\sim km/s) and slip velocities (\sim m/s) depend in particular on the temporal evolution of the shear stress along the fault during sliding (i.e., fault strength

weakening and re-strengthening) (Ida, 1972; Ruina, 1983). Friction experiments, performed with rotary shear machines designed to impose on rock specimens slip and slip rates typical of natural earthquakes, proved that experimental faults weakened due to several rock-type and environmental-dependent thermally activated weakening mechanisms, including melt lubrication, grain-size dependent processes, thermal and thermomechanical pressurization of pore fluids, etc. (Tsutsumi and Shimamoto, 1997; Di Toro et al., 2004; Han et al., 2010; Rice, 2006; Ferri et al., 2010; Di Toro et al., 2011; Green et al., 2015; De Paola et al., 2015; Spagnuolo et al., 2015; Violay et al., 2015). Field studies of exhumed natural seismogenic faults support the evidence of rapid weakening and fault lubrication during earthquakes (Sibson et al., 1975; Di Toro et al., 2006). The rheology of the fault is related to the physical state (e.g., liquid vs. solid) of the slipping zone (Rice, 2006), the slip rate and slip acceleration (Di Toro et al., 2004; Niemeijer et al., 2011; Chang et al., 2012), the rock composition (Di Toro et al., 2011; Goldsby and Tullis, 2011; Green et al., 2015), the presence of water (Violay et al., 2013, 2014a, 2014b), the ambient and local

* Corresponding author.

E-mail address: marie.violay@epfl.ch (M. Violay).

temperature (Lockner et al., 1986; Verberne et al., 2015), and in presence of non-cohesive rocks, on the gouge grain size (De Paola et al., 2015). Indeed, in cohesive rocks, slip is highly localized from the very initiation of sliding and the rise of the temperature in the slipping zone increases with slip rate, effective normal stress and square root of the duration of sliding (e.g., Rice, 2006; Aubry et al., 2018). In cohesive rocks, the abrupt increase in temperature favors “flash” heating and weakening mechanisms (Goldsby and Tullis, 2011) which may eventually evolve, for some silicate-built cohesive rocks, in bulk melting (Hirose and Shimamoto, 2005; Niemeijer et al., 2011; Violay et al., 2013; Aubry et al., 2018). On the contrary, in the presence of gouges, some slip is required before strain localization is achieved (Beeler and Tullis, 1996; Marone et al., 1990; Smith et al., 2015; Platt et al., 2014, 2015; Rice et al., 2014; Rempel et al., 2017). As a consequence, heat production is more distributed in the slipping zone and other processes including thermal (if fluids are already present in the pores of the slipping zone) and thermomechanical (if fluids like CO₂ and H₂O are released by the breakdown of the minerals of the slipping zone) pressurization might be favored before bulk melting of the slipping zone occurs (e.g., Rice, 2006; Segall and Rice, 2006; Brantut et al., 2008; Ferri et al., 2010; Acosta et al., 2018).

While the physical parameters controlling fault weakening have been extensively studied, little attention has been dedicated on the processes associated to frictional re-strengthening observed during slip deceleration in seismic velocity pulses (Del Gaudio et al., 2009; Chang et al., 2012; Liao et al., 2014; Proctor et al., 2014; Sone and Shimamoto, 2009). However, fault strength evolution, i.e. both strength weakening and re-strengthening, coupled with electrodynamic rupture propagation contributes actively to the slip rate evolution during seismic faulting and to the release of seismic waves (Sone and Shimamoto, 2009). In addition, co-seismic re-strengthening processes controls the energy budget of earthquakes, as well as the transition from crack-like to pulse-like rupture, which implies a strong fault re-strengthening after the passage of the rupture front (Beeler and Tullis, 1996). Few mechanisms of fault re-strengthening have been proposed so far: (1) temporal variation of stress conditions on the rupture interface during the passage of the rupture front (e.g., punctual pore fluid pressurization) (Lykotraftis et al., 2006), (2) spatial variation of the initial stress field (barrier model) (Peyrat et al., 2001; Latour et al., 2011), (3) high dependence of friction to sliding velocity, i.e., “self-healing” behavior during sliding velocity deceleration (Beeler and Tullis, 1996; Sone and Shimamoto, 2009; Proctor et al., 2014; Perrin et al., 1995; McLaskey et al., 2015; Zheng and Rice, 1998). Here, we present friction experiments that, by reproducing seismic slip conditions, aim at understanding the effect of rock composition and water content on fault re-strengthening during slip deceleration. In particular, we focused on cohesive rocks (calcitic marble and microgabbro) where strain is localized from slip initiation to the final re-strengthening stage and the temperature evolution in the slipping zone is simpler than in case for non-cohesive rocks (gouges). Moreover, the analysis of the data reported here exploit the achievement of the so-called “steady-state” shear stress conditions in the experiments. This achievement requires slips of several centimeters to tens of centimeters depending on the applied effective normal stress (Di Toro et al., 2011). Consequently, the results presented here should be valid for moderate to large in magnitude earthquakes, though steady-state conditions might not ever be achieved in nature (Liao et al., 2014). The experimental evidences suggest that rock composition and environmental conditions play a pivotal role in fault re-strengthening during seismic faulting, with dramatic consequences in the radiation pattern of the emitted seismic waves.

2. Methods

We performed 53 high speed friction experiments on hollow cylinders (30/50 mm internal/external diameter) of carbonate-built rock (Carrara marble, 99% calcite) and silicate-bearing rock (micro-gabbro) (for sample preparation, see Nielsen et al., 2012). Carbonate-built rocks and gabbros often host earthquakes sequences in nature, as attested by geological evidence (Sibson et al., 1975). The experiments were performed with SHIVA, a rotary shear machine installed at the HP-HT INGV laboratories in Rome (see sup.mat.Table 1). SHIVA was equipped with two brushless engines (max power 300 kW) and an air actuator (2000 kg amplified to 5000 kg thanks to a lever) in a rotary shear configuration to slide the two contacting hollow rock cylinders under the desired conditions (Di Toro et al., 2010). Experiments were performed either in the presence of pressurized liquid water, room humidity or under vacuum (10⁻⁴ mbar). In the experiments with liquid water, SHIVA was equipped with a pressurizing system which consisted of (1) a fluid pressure vessel (i.e., the samples were fully immersed in water), (2) a membrane pump with a 30 cm³ fluid capacity, (3) a pressure multiplier that imposes up to 15 MPa of fluid pressure (P_f), (4) a pressure regulator and, (5) valves and pipes (Violay et al., 2013). Normal stress (σ_n) and pore pressure (P_f) (drained conditions) were kept constant during experiments to target values ranging between 10 and 40 MPa and 0 (nominally dry) and 15 MPa, respectively. To mimic the sliding velocity at a given point of the fault during propagation and arrest of seismic slip, we imposed a trapezoidal slip velocity function by imposing constant acceleration and deceleration (7.8 m s⁻²) and target slip velocities ranging from 1 m s⁻¹ to 6.5 m s⁻¹. Total slip ranged from 0.83 m to 18.37 m.

Mechanical data (axial load, torque, axial displacement, and angular rotation) were acquired at a frequency up to 25 kHz (for description of the installed instrumentation, their calibration and acquisition rates, see Niemeijer et al., 2011). Normal stress, shear stress (τ) and slip velocity (V) were computed from experimental measurements following Tsutsumi and Shimamoto (1997) and Di Toro et al. (2010).

3. Results

In all the experiments, once the slip velocity function was applied, the apparatus and the sample initially deformed elastically until the static friction coefficient μ_p ($\mu = \tau/\sigma_n^{eff}$ with $\sigma_n^{eff} = \sigma_n - P_f$) was overcome and slip initiated (Fig. 1). Then, the friction coefficient decreased exponentially with slip over a weakening distance D_w down to a so-called steady-state friction coefficient μ_{ss} . Towards the end of the experiment, during slip velocity deceleration, the friction coefficient recovered with time and slip to a final value μ_r at the offset of slip (Figs. 1a–b). The effects of rock composition and environmental conditions on fault weakening and μ_p , μ_{ss} and D_w were discussed in Violay et al. (2013 and 2014a, 2014b). As well as for initial fault weakening (Di Toro et al., 2011), the recovery of the friction coefficient during the deceleration stage of the velocity pulse is a function of the sliding velocity (Figs. 1c–d) (Goldsby and Tullis, 2011; Passelègue et al., 2014; Proctor et al., 2014). The value of μ_r ranged from 0.08 to 0.63 for Carrara marble and 0.11 to 0.37 for micro-gabbro, respectively, and independently of (1) the environmental conditions, (2) the final slip and (3) of the initial power ($\sigma_n^{eff} V$) imposed on the fault (Figs. 2 and 3). To investigate the physics of the re-strengthening processes, we computed, for each experiment, the friction re-strengthening rate $\dot{\mu} = (\mu_r - \mu_{ss})/(t_r - t_{ss})$, where $(t_r - t_{ss})$ is the deceleration duration from end of the steady-state to the end of slip (Figs. 1a–b). At constant acceleration and deceleration rate, in the experiments conducted at low initial power density ($\sigma_n^{eff} V <$

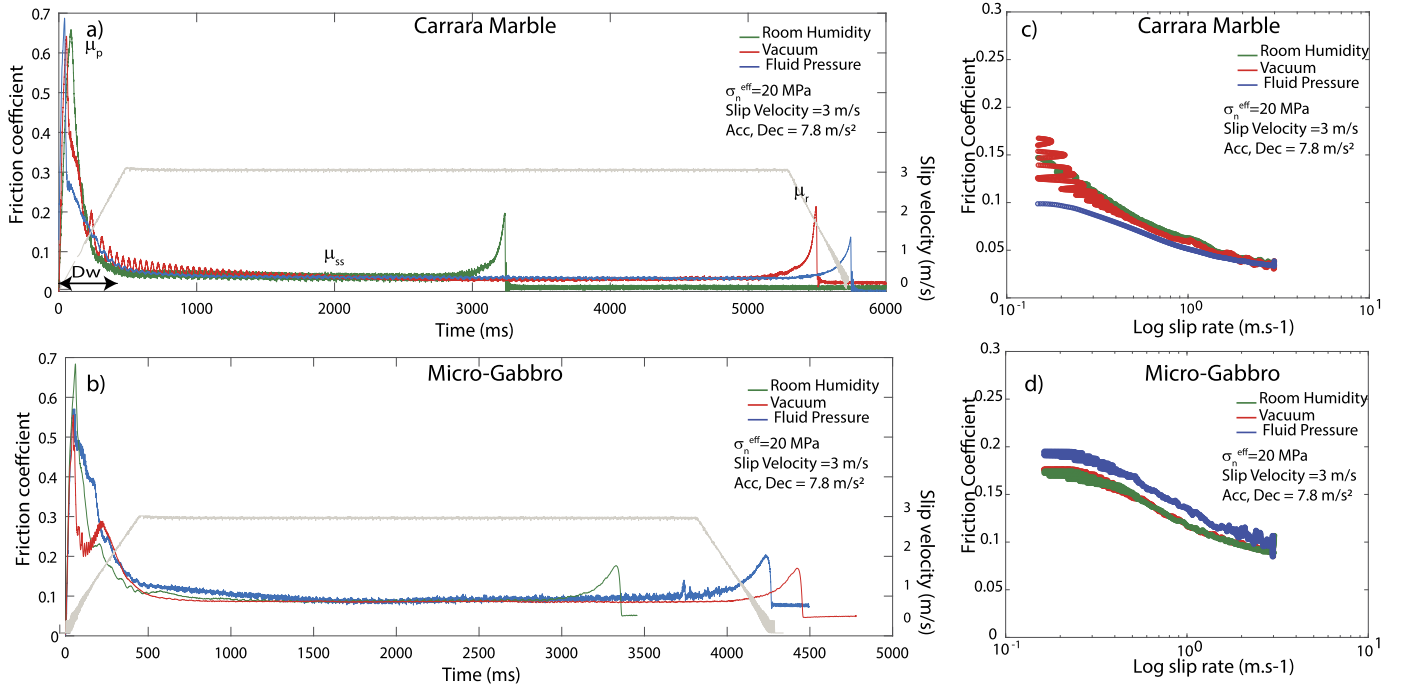


Fig. 1. Evolution of the friction coefficient with time and slip rate for Carrara marble and micro-gabbro slid at seismic slip rates. **(a) and (b)** Evolution of the friction coefficient with time in Carrara marble and micro-gabbro. **(c) and (d)** Evolution of the friction coefficient measured during deceleration versus log of the sliding velocity. The experiments were conducted at target velocity $V_t = 3 \text{ m s}^{-1}$, acceleration and deceleration $= 7.8 \text{ m s}^{-2}$, and $\sigma_n^{eff} = 20 \text{ MPa}$ (effective normal stress $= \sigma_n - P_f$). Blue curves (S615 and S567): fluid pressure experiments $\sigma_n = 25 \text{ MPa}$, $P_f = 5 \text{ MPa}$; green curves (S307 and S555): room humidity experiments; red curves (S614 and S585): vacuum experiments were run at $P_{vacuum} = 10^{-4} \text{ mbar}$. Two examples of sliding velocity function are drawn in grey. (For interpretation of the colors in the figure(s), the reader is referred to the web version of this article.)

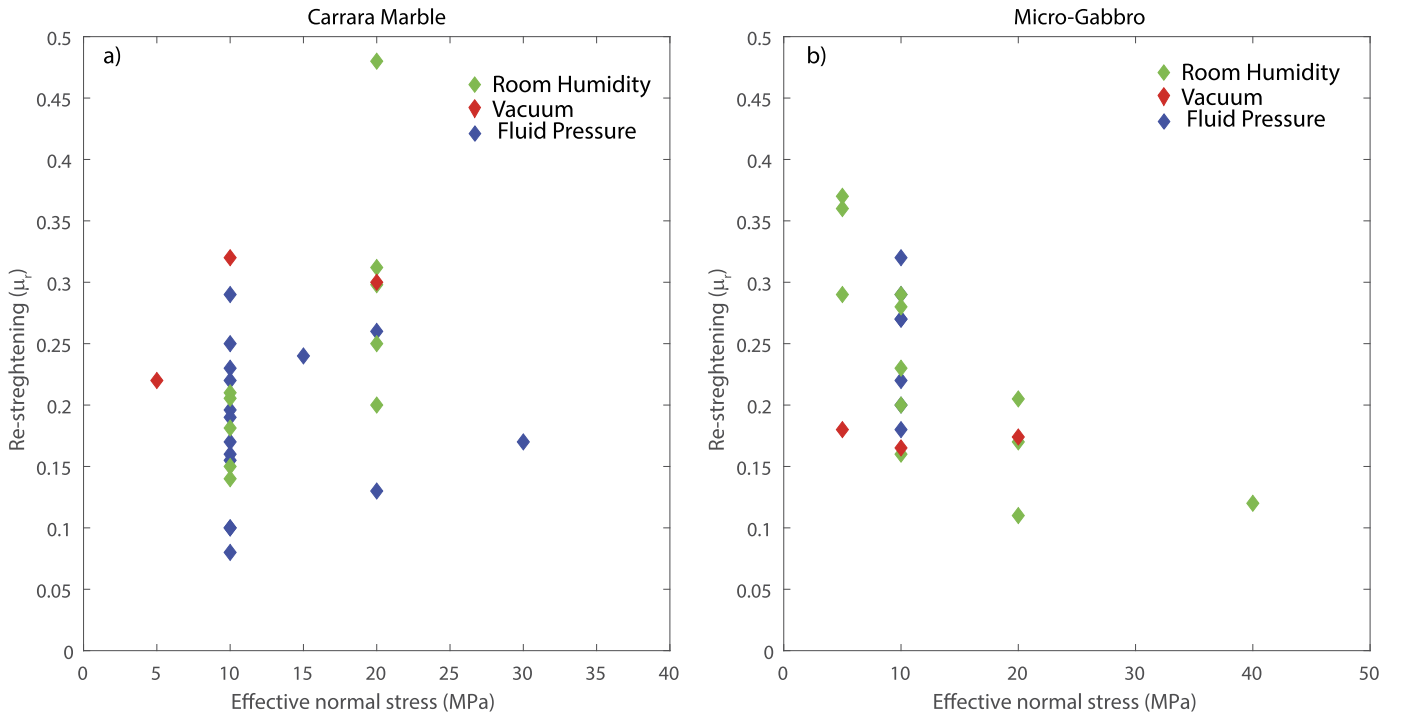


Fig. 2. Influence of σ_n^{eff} on the re-strengthening for **(a)** Carrara marble and **(b)** micro-gabbro. Blue dots: fluid pressure experiments; green dots: room humidity experiments; red dots: vacuum experiments $P_{vacuum} = 10^{-4} \text{ mbar}$.

20 MW m^{-2}) and under both room humidity and vacuum conditions, the re-strengthening rate was ~ 17 times faster in Carrara marble (from 2.00 to 3.68 s^{-1}) than in micro-gabbro (from 0.02 to 0.16 s^{-1}) (Fig. 4). In both rock types, re-strengthening rate was initial power density-dependent and work density independent (i.e.,

slip independent) (Fig. 4). In Carrara marble, independently of the environmental conditions, the friction re-strengthening rate decreased with increasing power density (Figs. 3–4). This trend was amplified in pressurized water conditions, and at the largest power densities tested, re-strengthening rate became almost negligible

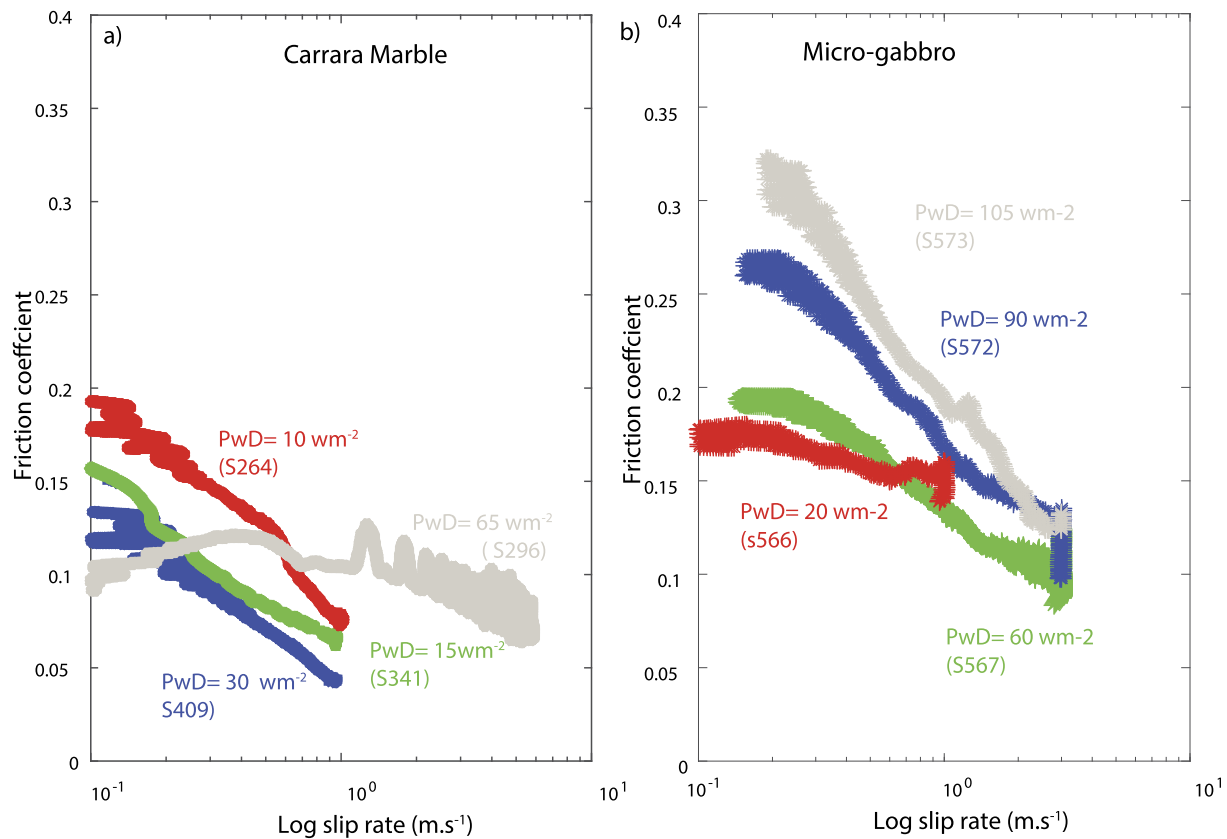


Fig. 3. Evolution of the friction coefficient during slip deceleration versus log of the sliding velocity for (a) Carrara marble (S409, S341, S296, S264) and (b) micro-gabbro (S566, S567, S572 and S573). Experiments were conducted at different power density ($\sigma_n^{eff} \cdot Vt$). Target velocity (Vt) ranging from 1 and 6.5 m s^{-1} , acceleration and deceleration = 7.8 m s^{-2} , and σ_n^{eff} from 10 to 30 MPa (effective normal stress = $\sigma_n - P_f$). The experiments were all performed under fluid pressure conditions ($P_f = 5$ MPa).

(Fig. 4a). The opposite behavior was observed in micro-gabbro. The re-strengthening rate slightly increased with the power density, and this effect was amplified in presence of pressurized water (Fig. 4b). Moreover, in Carrara marble the re-strengthening rate was about two times (at low power density) slower in the presence of pressurized liquid water than under room and vacuum conditions (Fig. 4). Instead, in micro-gabbro, the frictional re-strengthening rate was about three times faster in the presence of pressurized liquid water than under room humidity and vacuum conditions (Fig. 4). Therefore, pressurized liquid water had an opposite effect on the frictional re-strengthening rate of Carrara marble with respect to the one of micro-gabbro.

Regarding the microstructures, mineralogy and geochemistry of the slipping zones and slip surfaces recovered after the experiments, we refer to previous studies performed (1) on several samples from the experiments presented here (Violay et al., 2013, 2014a, 2014b) and (2) on slipping zone produced in experiments conducted on similar rocks (e.g., gabbro, basalts and Carrara marbles) under very similar deformation conditions (Han et al., 2010; Di Toro et al., 2011). In the case of micro-gabbro, the slipping zone consisted of a continuous ca. 200 μm thick layer of a quenched melt (see composition in Table 2), independently of the presence or absence of liquid water (Fig. 5a) (Violay et al., 2014a, 2014b, 2015; Nielsen et al., 2008, 2010; Niemeijer et al., 2011; Giacomel et al., 2018). In the case of the Carrara marble, the slipping zone after experiments conducted under vacuum and room humidity consisted of a 50 to 100 μm thick layer of nano- to micro-grained, poorly cohesive material made of calcite and, to a minor extent, lime (Violay et al., 2013; Spagnuolo et al., 2015) (Fig. 5b). Unfortunately, due to the poorly cohesive nature of the nano- to micro-grained deformed layer, most of the slipping zone was flushed

away during sample recovery in the experiments performed in the presence of liquid water. However, the few micro-fault patches recovered from the slip surface showed the presence of nano- to micro-grained slipping zones (Violay et al., 2013, 2015) and evidence of calcite decarbonation attested by the presence of vacuoles within the grains. Violay et al. (2013) also showed evidence of CO_2 increase in the fluids recovered after high-speed friction experiments performed on carbonate bearing rocks. We infer that also in the case of the experiments performed with Carrara marble, the slipping had the same microstructure independently of the presence or absence of liquid water.

4. Discussion

4.1. Effect of water on friction re-strengthening rate

The different effect of the presence of pressurized liquid water on the frictional re-strengthening rate of micro-gabbro and Carrara marble suggested that different micro-physical processes operated during the deceleration phase of the slip pulse, as clearly supported by microstructural evidence (Fig. 5). It is well-known that fault surfaces of micro-gabbro melt with seismic slip under room humidity and vacuum conditions (Tsutsumi and Shimamoto, 1997; Hirose and Shimamoto, 2005; Nielsen et al., 2008; Niemeijer et al., 2011), but also in the presence of liquid water (Violay et al., 2014a, 2014b). On the contrary, slipping zones of Carrara marble did not record microstructural evidence of frictional melting. Instead, the slipping zones were made of sub-micrometer to nanometer in size grains (Spagnuolo et al., 2015). These microstructures can be associated to grain-size dependent crystal plastic processes (Green et al., 2015; De Paola et al., 2015; Spagnuolo et al., 2015). Similarly to

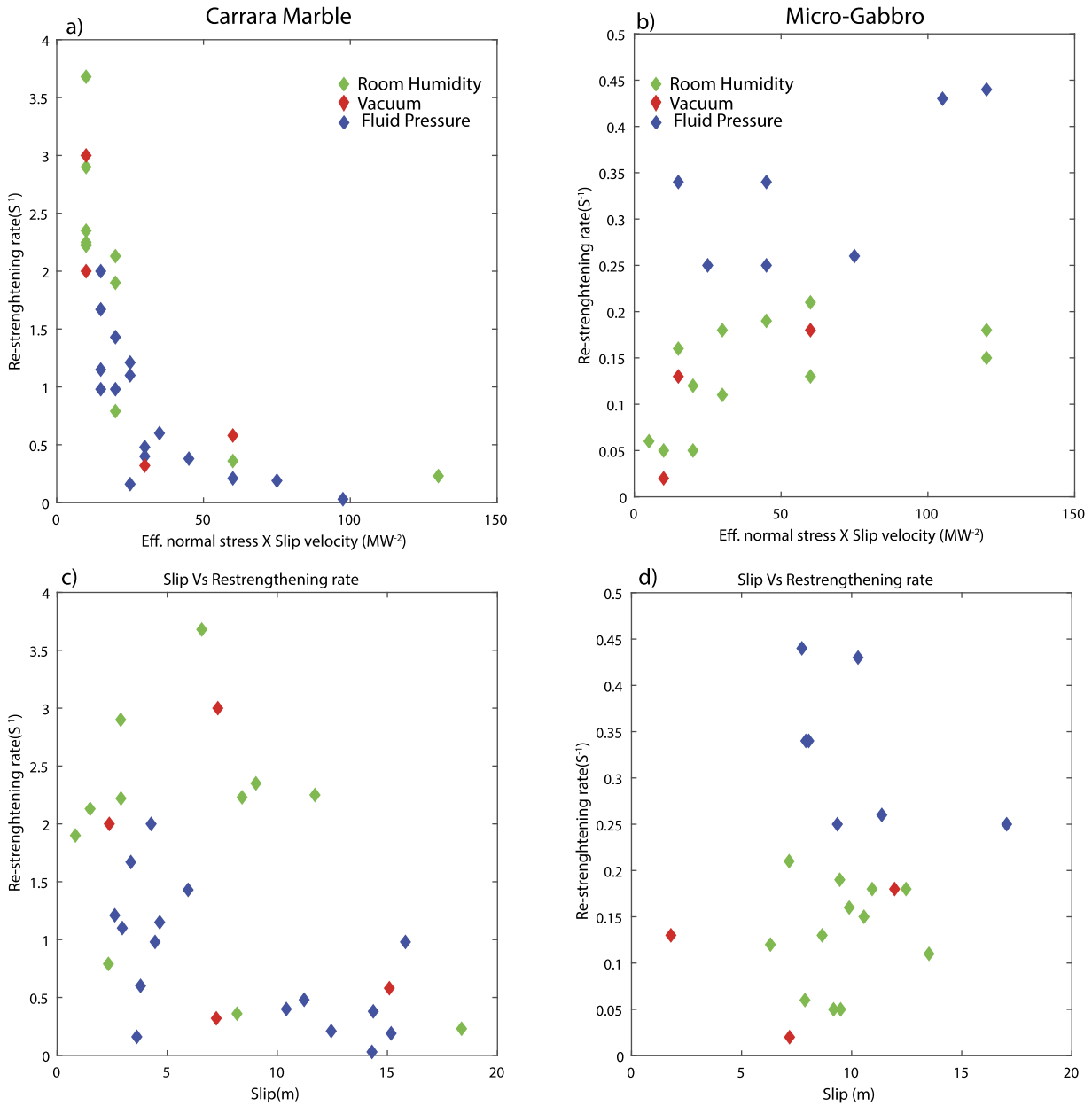


Fig. 4. Influence of power density (a, b) ($\sigma_n^{eff} \cdot Vt$) and slip (c, d) on the friction re-strengthening rate. Blue dots: fluid pressure experiments; green dots: room humidity experiments; red dots: vacuum experiments $P_{vacuum} = 10^{-4}$ mbar.

Table 1

Thermal properties of the fluid (air and water) and micro-gabbro used in the FEM numerical model, as well as the thermal properties of Carrara marble used for the coupled diffusion model and plasticity flow law. K = thermal conductivity, ρ = density, C = specific heat. Φ the liquid fraction.

	Micro-gabbro	Carrara marble	Water	Air	Melt	Steel
K [10^{-6} m ² /s]	0.8	1.48	0.15	1.5	0.344	4.2
ρ [kg/m ³]	2990	2700	1000	1.2	2591	2000
C [J/(kg K)]	949	700	4200	1000	1484	460

what occurred during the initial weakening stage, was the rheology of the materials building the slipping zone that controlled the final frictional re-strengthening. In our experiments, the rheology of the slipping zone depended on the physical state of the sheared materials (melt vs. nano-grains), on the slip and strain rate, on the normal stress, as well as on the environmental conditions and, for Carrara marble, on grain size.

In the case of micro-gabbro, the viscosity and thickness of the melt layer and its extrusion rate from the slipping zone controlled the viscous strength of the experimental fault (Nielsen et al., 2008). Violay et al. (2014a) showed that the initial fault weakening by frictional melts was delayed by the presence of liquid water that cools the asperity contacts. Here, we hypothesize that frictional re-strengthening might be enhanced by an increase of the viscous strength of the melt layer due to water-cooling. To test this hypothesis, we implemented a Finite Element Methods numerical model which included the rock specimens and the steel-made pressure vessel (Fig. 6a, b, c). The slipping zone was modeled as a 200 μ m-thick layer (red in color in Fig. 6, a), consistently with the typical thickness of the solidified melt layers recovered at the end of the experiments (Nielsen et al., 2008), made by melt plus water or melt plus air with a constant volume ratio (ϕ) ranging from 0.5 to 0.9 in agreement with microstructural observations (Brown and Fialko, 2012; Violay et al., 2014a, 2014b) (Fig. 5). The melt

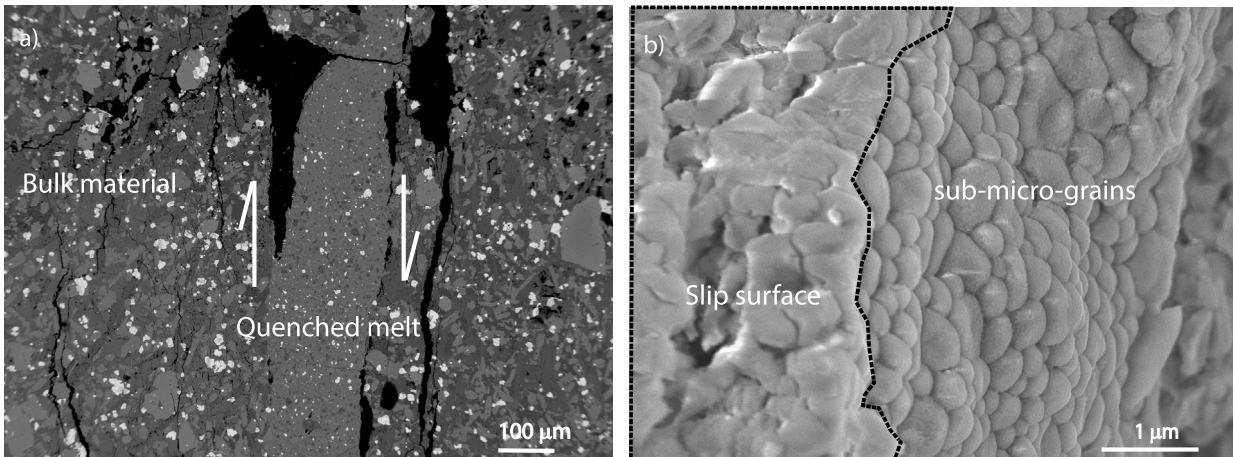


Fig. 5. Microstructural observations of experimental slip surfaces and slipping zones after shearing. **(a)** Slipping zone after an experiment performed on micro-gabbro (s585, $V = 3 \text{ m s}^{-1}$, $\sigma_n = 20 \text{ MPa}$, Vacuum conditions see also Violay et al., 2014a, 2014b). The slipping zone is made by quenched melt (i.e., glass matrix, see composition in Table 2) which wraps grains of plagioclase and pyroxene that survived from frictional melting (Scanning Electron Microscope, back scatter electron image). **(b)** Slip surface after an experiment performed on calcitic Carrara marble (s614, $V = 3 \text{ m s}^{-1}$, $\sigma_n = 20 \text{ MPa}$, Vacuum conditions, see Violay et al., 2014a, 2014b). The slip surface is made by micro- to nano-grains of calcite and lime. Small decarbonation vacuoles decorate the recrystallized calcite grains (Scanning Electron Microscope, secondary electron image).

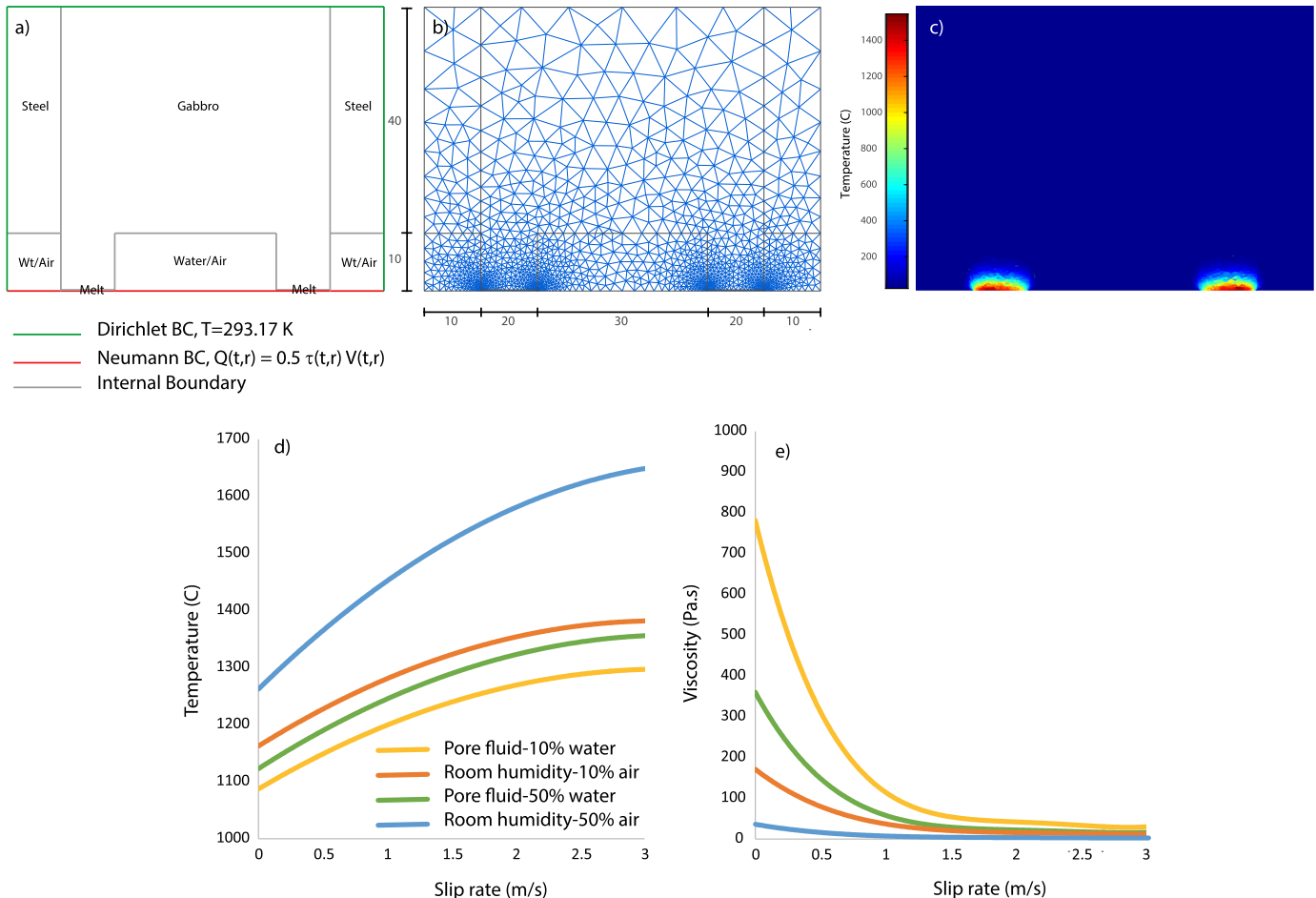


Fig. 6. FEM 2D time dependent heat diffusion model. **(a, b)** Model geometry with description of the boundary conditions and mesh geometry. **(c)** The snapshot of the temperature distribution at the end of the experiment s585 conducted on gabbro. **(d)** Temperature evolution of the slip zone during slip deceleration ($t_r - t_{ss}$). **(e)** Melt viscosity evolution during slip deceleration.

temperature during slip deceleration was computed using the mechanical data of the samples sheared under vacuum conditions as a reference. In fact, under vacuum conditions, most of the frictional work was dissipated into heat (the contribution to wear and rock

fragmentation was negligible, see Niemeijer et al., 2011) and very limited heat was lost by radiation. Consequently, the heat flux Q was a function of shear stress and slip rate that evolved with time t (Fig. 1) and varied along the sample radius r :

$$Q(r, t) = 0.5 \cdot \tau(t) \cdot V(r, t). \quad (1)$$

For experiments performed under room humidity conditions and in the presence of water, we imposed that the melt layer was cooled by air or water (2D heat diffusion model), respectively. Then, as representative of the entire slipping zone, we used the estimated temperature achieved by the friction melt at 2/3 of the sample radius. The properties of the slipping zone (indicated by the subscript $_{eff}$ for effective) were considered as a linear combination of the thermal properties of the fluid (air or water) and those of the melt (Table 1). Therefore, the “effective” thermal diffusivity in the slip zone was:

$$\alpha_{eff} = K_{eff}/(\rho C)_{eff} \quad (2)$$

where

$$K_{eff} = (1 - \phi)K_R + \phi K_f \quad (3)$$

and

$$(\rho C)_{eff} = (1 - \phi)\rho_R C_R + \phi \rho_f C_f \quad (4)$$

with K , the thermal conductivity ($\text{W m}^{-1} \text{K}^{-1}$), C the specific heat capacity ($\text{J kg}^{-1} \text{K}^{-1}$), ρ the density (kg m^{-3}) and ϕ the liquid fraction in the melt. Index R and f are related to the rock and fluid properties, respectively. Then, the heat diffusion is:

$$\rho C_{eff} \frac{\partial T}{\partial t} = \nabla(k_{eff,i} T) \quad (5)$$

where i represents the two different materials (water/air and rock) in the model of Fig. 6. Values of thermal conductivity, specific heat capacity and density are reported in Table 1. The melt viscosity (η) was computed with the viscosity simulator for silicate melts of Giordano et al. (2008) (we did not take into account the crystal fraction in the melt). The model predicts the non-Arrhenius temperature dependence of viscosity for naturally-occurring silicate melts at atmospheric pressure:

$$\log(\eta) = A + \frac{B}{T(K) - C} \quad (6)$$

where A is a constant independent of composition and B and C are adjustable parameters depending on melt composition. The glass chemical composition was published by Violay et al. (2014a, 2014b, sup mat item 4) and reported in Table 2. Numerical modeling results highlighted that the melt viscosity, because of cooling of the melt, increases with decreasing sliding velocity (Fig. 6), in agreement with the logarithmic increase of the “friction coefficient” during the deceleration stage (Figs. 1 and 3). In addition, the increase of melt viscosity during slip deceleration was significantly faster in experiments performed in the presence of pressurized water than under room humidity conditions, suggesting that water-cooling was an efficient mechanism of re-strengthening. Moreover, the efficiency of water-cooling was proportional to the fluid-to-melt ratio in the slipping zone, and therefore of the temperature of the melt before deceleration. Indeed, higher was the melt temperature at the steady-state, which was slightly proportional to the imposed power density, faster was the increase of melt viscosity during slip deceleration. Instead, given the same conditions, the observation that the re-strengthening rate was independent of slip (Figs. 4d) was related to the large shortening rate of the rock specimens during frictional melting (mm per meters of slip, Violay et al., 2014a, 2014b). At steady-state conditions, the isotherms were almost fixed in space while the rock specimen passes through them and got melted and extruded (see discussion in Nielsen et al., 2008). As a consequence, once steady-state

Table 2

Chemical composition of the micro-gabbro (XRD) and of the glass for experiment S585 performed under vacuum conditions (Electron Microprobe Analysis). The analysis does not close to about 100% because only Fe^{2+} was determined.

Sample Phase #	Micro-gabbro crystalline	s585 glass #	s.d.
Al_2O_3	14.27	15.68	0.74
Na_2O	4.49	4.26	0.91
CaO	9.22	10.21	1.43
SiO_2	45.48	45.22	0.90
K_2O	2.71	2.71	0.57
MgO	7.15	6.88	0.57
P_2O_5	1.88	1.14	0.14
FeO	10.28	8.31	0.34
TiO_2	3.02	2.88	0.38
MnO	0.19	0.17	0.05
Total	98.69	97.46	

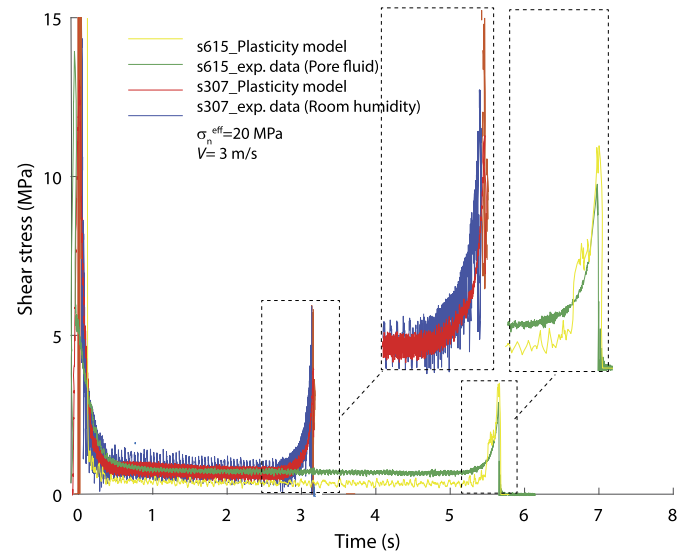


Fig. 7. Results of the 1D time dependent heat diffusion model fully coupled with diffusion creep flow law for both room humidity (blue and red curves) and pore fluid (green and yellow curves) conditions.

had been achieved (always the case for the experiments presented here), during deceleration and melt cooling, the wall rocks were at similar temperatures independently of the cumulated slip and the re-strengthening is independent of slip.

In the case of Carrara marble, the slower re-strengthening rate in the presence of water than under room humidity conditions (Fig. 4a) cannot be explained by water cooling of the slipping zone or by thermal fluid depressurization (i.e., fluid pressure decrease after a short period of expansion caused by frictional heating). Indeed, neither melt was produced nor pressurization was observed during these experiments where fluid pressure was kept constant under drained conditions (Violay et al., 2015). Moreover, both melt lubrication and thermal pressurization would lead to a faster re-strengthening in presence of water than under room humidity conditions. However, this is at odds with the experimental evidence: re-strengthening rate is faster under vacuum conditions (Fig. 4). Note also that calcite decarbonation as potential re-strengthening mechanism can be ruled out in our experiments. This mechanism would lead to faster re-strengthening at high power density (i.e., higher temperature), which it is just the opposite of our experimental evidence.

We suggest that the slower recovery of the frictional strength in the presence of liquid water during slip deceleration can be due to the strain rate sensitive, grain size dependent crystal plastic-

ity of calcite in the presence of water (e.g., grain boundary sliding aided by diffusion creep) (Rutter, 1974; Schmidt et al., 1980, 1987; Walker et al., 1990; Renner et al., 2002). Decarbonation reaction can probably help this mechanism because it triggers the formation of nanoparticles allowing the activation of grain size dependent processes. Despite relevant differences between our experimental protocol and those reported in the above-mentioned studies (high pressure – high temperature triaxial tests performed at very low strain rates, 10^{-6} – 10^{-4} s $^{-1}$, compared to those achieved in our experiments, 10^2 – 10^4 s $^{-1}$), a comparison with those studies may help to understand better the mechanisms accommodating deformation in our experiments. At high temperature (>400 °C), calcite strength is temperature and strain rate dependent (Rutter, 1972, 1974), and governed by crystal-plastic and grain size-dependent deformation mechanisms (intracrystalline plasticity and grain boundary sliding diffusion-assisted plasticity). Similar deformation mechanisms were inferred to be operating at sub-seismic and seismic slip rates in calcite (Verberne et al., 2015; De Paola et al., 2015; Spagnuolo et al., 2015). Rutter (1972) showed that calcite strength is inversely proportional to water content due to the reduction of the surface energy at calcite grain boundaries (Boozier et al., 1963) and its strain rate sensitive behavior decreased with increasing water content. Rutter (1974) had also shown that water effect is relatively small in Carrara marble. If crystal-plastic and grain-size dependent processes were triggered during high velocity friction experiments, they would therefore result in a negative dependence of strain-rate on residual flow stress, and may explain the inhibition of the frictional re-strengthening in Carrara marbles especially at large power densities. In fact, for larger power densities, higher temperatures should be achieved in both the slipping zone and wall rocks. This should be the case especially once the so-called steady-state conditions were achieved (note that, because of the power-law decay in Carrara marble, “steady-state” conditions remain an approximation, see Nielsen et al., 2016). In fact, because of the absence or negligible shortening of the marble specimens, contrary to what happens in micro-gabbro, heat diffused in the wall rocks. Hotter wall rocks and the different deformation mechanism involved would result in slower cooling of the slipping zone, especially if compared to the frictional melting case (compare Fig. 4a with 4b). In the presence of water, the efficiency of grain size dependent and diffusion-controlled processes should be enhanced due to lower activation energy in presence of water, explaining the lower re-strengthening rate. However, the slipping zone was flushed away at the end of slip preventing sample recovery for micro-analytical investigations (Violay et al., 2013, 2014a, 2014b). To test this hypothesis, we performed a one dimension-time dependent diffusion temperature model fully coupled with grain-size diffusion creep flow law (Fig. 7). Calcite thermal properties are reported on Table 1. The slipping zone was modeled by a 100 μ m – layer composed of 100 nm grain size calcite, in agreement with microstructural observations (Violay et al., 2013, 2015) (Fig. 5). The heat flux and diffusion were computed following Eqs. (1) and (5). The predicted flow stress for diffusion creep plasticity can be modeled by the constitutive flow law (Eqs. (8), (9)).

$$\frac{\partial V}{\partial t} = \frac{1}{2} \tau(t) V(t) + \frac{k}{C_p \rho} \frac{\partial^2 T}{\partial x^2} \quad (7)$$

$$\tau(t) = \left(\frac{\dot{\gamma}}{A \cdot D^{-b} e^{-\frac{H}{RT(t)}}} \right) \quad (8)$$

$$\dot{\gamma} = \frac{1}{l} \frac{\partial V}{\partial t} \quad (9)$$

where $\dot{\gamma}$ is the shear strain rate, A the pre-exponential factor, H the apparent activation energy for creep, R the gas constant, T the temperature, τ the shear stress at time step (t), n the stress exponent, D the grain size with b the grain size exponent, l is the layer thickness, and $V(t)$ is the slip velocity function.

Following (De Paola et al., 2015), under room-humidity conditions, $b = 2$, $n = 1$, $H = 217$ kJ mol $^{-1}$, $A = 9.55 \times 10^5$ (s $^{-1}$ Bar $^{-n}$), $R = 8.314$ J K mol $^{-1}$. In presence of water, we supposed a reduction of the activation energy (H) of about 20%, with $H = 176$ K J kJ mol $^{-1}$ (see discussion in Rutter, 1972). Flow stress estimates based on Eqs. (7), (8), (9) (Fig. 7) showed that grain boundary sliding aided by diffusion mechanism can explained both the strength weakening at the beginning of the experiments, the steady state friction and the final re-strengthening. Moreover, a decrease of the activation energy of only 20% under pore fluid conditions (Rutter, 1972) may justify the faster re-strengthening observed under dry rather than under pore fluid conditions (Fig. 1c).

4.2. Implications for natural earthquakes

Our experiments demonstrated that the slip deceleration can result in rapid fault re-strengthening, up to 10 to 90% of the initial peak stress, depending on the rheology of the material building the slip zone which depends on lithology and environmental conditions (Fig. 1). Because the friction coefficient is strongly velocity-dependent (Sone and Shimamoto, 2009), the magnitude of the re-strengthening depends mainly on the imposed deceleration rate (Del Gaudio et al., 2009). The extrapolation of these results to natural earthquakes can be gained by (1) comparing the friction re-strengthening rate between experiments performed with different rock types and under environmental conditions, and (2) using the dependency of the re-strengthening rate with the power density.

Here below, we estimate the slip-velocity, acceleration and power density of natural earthquakes and compare them to the imposed parameters during our experiments. Slip-velocity functions during earthquake rupture propagation are obtained by inverting ground motion waveforms. Slip acceleration and deceleration during earthquakes are ~ 1 – 10 ms $^{-2}$ (and larger, Tinti et al., 2005) and slip rates, on average, ~ 1 ms $^{-1}$ (Heaton, 1990). Therefore, acceleration, deceleration as well as slip-velocity imposed in our experiments are somehow comparable to those of natural earthquakes. The main differences between tests and earthquakes are in the shape of the velocity function (trapezoidal in our case) and on the normal stress imposed. Indeed, crustal earthquakes nucleate between 5 and 15 km depth, possibly at effective normal stresses of ~ 100 – 200 MPa (Zoback and Harjes, 1997), and at power densities perhaps up to ten times higher than those imposed in the experiments discussed here. Extrapolation of our results to realistic stresses conditions suggest that in cohesive carbonate-bearing rocks, frictional re-strengthening during slip-velocity deceleration is probably almost negligible whereas in cohesive silicate bearing-rocks, re-strengthening processes are highly deceleration-dependent, especially in the presence of water.

Indeed, our results demonstrate that, due to the large expected power densities during natural earthquakes, small variations in the slip velocity could induce strong variations in friction promoting further changes in the slip velocity history due to co-seismic re-strengthening, especially in the case of calcite-built rocks. Moreover, the frequency content of the radiated energy is affected by the abruptness of velocity changes (emission of higher frequency waves is expected under abrupt decelerations) and thus, by the re-strengthening rate. Based on our results, cohesive silicate-bearing faults that undergo to frictional melting, also in the presence of liquid water (see natural case discussed by Brantut and Mitchell, 2018) will have the largest re-strengthening rates at the highest

power densities (5–15 km depth) and should promote more intense high frequency radiation during slip deceleration. However, according to Fig. 4, the re-strengthening rates in micro-gabbro are much smaller than those achieved in calcitic-built cohesive rocks. In the latter rocks, if grain-size dependent processes are activated, intense high frequency radiation should occur especially at low power densities (perhaps corresponding to shallow depths, <2 km) and dry conditions, when re-strengthening rates are the highest (Fig. 4).

5. Conclusions

We performed a series of experiments simulating seismic slip under different environmental conditions (vacuum, room humidity and pressurized water) on two common cohesive crustal rocks (calcitic Carrara marble and micro-gabbro). In general, independently of the environmental conditions, the fault re-strengthening rate at the end of slip is up to one order of magnitude larger in Carrara marble than in micro-gabbro, especially at low power densities (Fig. 4). This large difference in re-strengthening rates is due to the different on-fault deformation processes operating during seismic slip: crystal plastic and grain-size dependent for Carrara marble, melt lubrication for micro-gabbro. The two deformation mechanisms have different constitutive equations and dependence with temperature. With increasing power density, which may correspond to increasing crustal depths, the fault re-strengthening rate becomes almost negligible for Carrara marble whereas it slightly increases for micro-gabbro.

We also found some intriguing second order differences in the magnitude of the re-strengthening rate for the two rock types. These differences are due to the environmental conditions which impact on the efficiency of the particular co-seismic deformation mechanism of the rock. Under vacuum and room-humidity conditions, fault re-strengthening rate at the end of simulated seismic slip in Carrara marble is significantly faster than in the presence of pressurized water, especially at low power densities (Fig. 4). Instead, in micro-gabbro, fault re-strengthening rate is faster in the presence of pressurized water than under room humidity and vacuum conditions (Fig. 4). We interpreted these well-reproducible second order variations in the re-strengthening rate as the consequence of the change in rate-dependent plasticity in the presence of water for Carrara marble and water-cooling of the frictional interface for micro-gabbro. Our results suggest that both rock composition and presence of water affect the elastic strain energy release rate and the seismic waves radiation pattern during rupture propagation.

Acknowledgements

This work was funded by the European Research Council Starting Grant project 757290-BEFINE and Consolidator Grant 614705 NOFEAR. We are grateful to S. Nielsen for scientific discussions. M.V. thanks Jean-Paul Violay for the discussions and help. We thank P.G. Scarlato for laboratory support. Raw data can be found at <https://zenodo.org/> or requested from the corresponding author at marie.violay@epfl.ch.

Appendix A. Supplementary material

Supplementary material related to this article can be found online at <https://doi.org/10.1016/j.epsl.2019.06.027>.

References

- Acosta, M., Passetlègue, F.X., Schubnel, A., Violay, M., 2018. Dynamic weakening during earthquakes controlled by fluid thermodynamics. *Nat. Commun.* 9 (1), 3074.
- Aubry, J., Passetlègue, F.X., Deldicque, D., Girault, F., Marty, S., Lahfid, A., et al., 2018. Frictional heating processes and energy budget during laboratory earthquakes. *Geophys. Res. Lett.* 45 (22), 12–274.
- Andrews, D.J., 2005. Rupture dynamics with energy loss outside the slip zone. *J. Geophys. Res., Solid Earth* 110 (B1).
- Beeler, N.M., Tullis, T.E., 1996. Self-healing slip pulses in dynamic rupture models due to velocity-dependent strength. *Bull. Seismol. Soc. Am.* 86 (4), 1130–1148.
- Booser, G.D., Hiller, K.H., Serdengecti, S., 1963. Effects of pore fluids on the deformation behavior of rocks subjected to triaxial compression. In: *Proc. Fifth Sympos. Rock Mechanics*. Univ. Minnesota.
- Brantut, N., Mitchell, T.M., 2018. Assessing the efficiency of thermal pressurization using natural pseudotachylite-bearing rocks. *Geophys. Res. Lett.* 45 (18), 9533–9541.
- Brantut, N., Schubnel, A., Rouzaud, J.N., Brunet, F., Shimamoto, T., 2008. High-velocity frictional properties of a clay-bearing fault gouge and implications for earthquake mechanics. *J. Geophys. Res., Solid Earth* 113 (B10).
- Brown, K.M., Fialko, Y., 2012. ‘Melt welt’ mechanism of extreme weakening of gabbro at seismic slip rates. *Nature* 488 (7413), 638.
- Brune, J.N., 1970. Tectonic stress and the spectra of seismic shear waves from earthquakes. *J. Geophys. Res.* 75 (26), 4997–5009.
- Chang, J.C., Lockner, D.A., Reches, Z., 2012. Rapid acceleration leads to rapid weakening in earthquake-like laboratory experiments. *Science* 338 (6103), 101–105.
- De Paola, N., Holdsworth, R.E., Viti, C., Collettini, C., Bullock, R., 2015. Can grain size sensitive flow lubricate faults during the initial stages of earthquake propagation? *Earth Planet. Sci. Lett.* 431, 48–58.
- Del Gaudio, P., Di Toro, G., Han, R., Hirose, T., Nielsen, S., Shimamoto, T., Cavallo, A., 2009. Frictional melting of peridotite and seismic slip. *J. Geophys. Res., Solid Earth* 114 (B6).
- Di Toro, G., Goldsby, D.L., Tullis, T.E., 2004. Friction falls towards zero in quartz rock as slip velocity approaches seismic rates. *Nature* 427 (6973), 436.
- Di Toro, G., Hirose, T., Nielsen, S., Pennacchioni, G., Shimamoto, T., 2006. Natural and experimental evidence of melt lubrication of faults during earthquakes. *Science* 311 (5761), 647–649.
- Di Toro, G., Han, R., Hirose, T., De Paola, N., Nielsen, S., Mizoguchi, K., et al., 2011. Fault lubrication during earthquakes. *Nature* 471 (7339), 494.
- Di Toro, G., Niemeijer, A., Tripoli, A., Nielsen, S., Di Felice, F., Scarlato, P., et al., 2010. From field geology to earthquake simulation: a new state-of-the-art tool to investigate rock friction during the seismic cycle (SHIVA). *Rend. Lincei* 21 (1), 95–114.
- Ferri, F., Di Toro, G., Hirose, T., Shimamoto, T., 2010. Evidence of thermal pressurization in high-velocity friction experiments on smectite-rich gouges. *Terra Nova* 22 (5), 347–353.
- Giacomel, P., Spagnuolo, E., Nazzari, M., Marzoli, A., Passetlègue, F., Youbi, N., Di Toro, G., 2018. Frictional instabilities and carbonation of basalts triggered by injection of pressurized H₂O- and CO₂-rich fluids. *Geophys. Res. Lett.* 45 (12), 6032–6041.
- Goldsby, D.L., Tullis, T.E., 2011. Flash heating leads to low frictional strength of crustal rocks at earthquake slip rates. *Science* 334 (6053), 216–218.
- Green, H.W., Shi, F., Bozhilov, K., Xia, G., Reches, Z., 2015. Phase transformation and nanometric flow cause extreme weakening during fault slip. *Nat. Geosci.* 8, 484–489.
- Han, R., Hirose, T., Shimamoto, T., 2010. Strong velocity weakening and powder lubrication of simulated carbonate faults at seismic slip rates. *J. Geophys. Res., Solid Earth* 115 (B3).
- Heaton, T.H., 1990. Evidence for and implications of self-healing pulses of slip in earthquake rupture. *Phys. Earth Planet. Inter.* 64 (1), 1–20.
- Hirose, T., Shimamoto, T., 2005. Growth of molten zone as a mechanism of slip weakening of simulated faults in gabbro during frictional melting. *J. Geophys. Res., Solid Earth* 110 (B5).
- Ida, Y., 1972. Cohesive force across the tip of a longitudinal-shear crack and Griffith’s specific surface energy. *J. Geophys. Res.* 77 (20), 3796–3805.
- Kanamori, H., Rivera, L., 2013. Energy partitioning during an earthquake. In: *Abercrombie, R., McGarr, A., Di Toro, G., Kanamori, H. (Eds.), Earthquakes: Radiated Energy and the Physics of Faulting*.
- Liao, Zonghu, Chang, Jefferson C., Reches, Ze’ev, 2014. Fault strength evolution during high velocity friction experiments with slip-pulse and constant-velocity loading. *Earth Planet. Sci. Lett.* 406, 93–101.
- Latour, S., Campillo, M., Voisin, C., Ionescu, I.R., Schmedes, J., Lavallée, D., 2011. Effective friction law for small-scale fault heterogeneity in 3D dynamic rupture. *J. Geophys. Res., Solid Earth* 116 (B10).
- Lockner, D.A., Summers, R., Byerlee, J.D., 1986. Effects of temperature and sliding rate on frictional strength of granite. In: *Friction and Faulting*. Birkhäuser, Basel, pp. 445–469.
- Lykotrafitis, G., Rosakis, A.J., Ravichandran, G., 2006. Self-healing pulse-like shear ruptures in the laboratory. *Science* 313 (5794), 1765–1768.
- Madariaga, R., 1976. Dynamics of an expanding circular fault. *Bull. Seismol. Soc. Am.* 66 (3), 639–666.
- Madariaga, R., Olsen, K.B., 2002. Earthquake dynamics. *Int. Geophys. Ser.* 81 (A), 175–194.
- Marone, C., Raleigh, C.B., Scholz, C.H., 1990. Frictional behavior and constitutive modeling of simulated fault gouge. *J. Geophys. Res., Solid Earth* 95 (B5), 7007–7025.

- Marty, S., Passelègue, F.X., Aubry, J., Bhat, H.S., Schubnel, A., Madariaga, R., 2019. Origin of high-frequency radiation during laboratory earthquakes. *Geophys. Res. Lett.*
- McLuskey, G.C., Kilgore, B.D., Beeler, N.M., 2015. Slip-pulse rupture behavior on a 2 m granite fault. *Geophys. Res. Lett.* 42 (17), 7039–7045.
- Nielsen, S., Di Toro, G., Hirose, T., Shimamoto, T., 2008. Frictional melt and seismic slip. *J. Geophys. Res., Solid Earth* 113 (B1).
- Nielsen, S., Spagnuolo, E., Smith, S.A.F., Violay, M., Di Toro, G., Bistacchi, A., 2016. Scaling in natural and laboratory earthquakes. *Geophys. Res. Lett.* 43 (4), 1504–1510.
- Nielsen, S., Spagnuolo, E., Violay, M., 2012. The Ultimate Sample Preparation for Rotary Shear Experiments. *Rapporti tecnici INGV*. <http://istituto.ingv.it/l-ingv/produzione-scientifica/rapporti-tecnici-ingv/numeri-pubblicati-2012>.
- Nielsen, S., Toro, G.D., Griffith, W.A., 2010. Friction and roughness of a melting rock surface. *Geophys. J. Int.* 182 (1), 299–310.
- Niemeijer, A., Di Toro, G., Nielsen, S., Di Felice, F., 2011. Frictional melting of gabbro under extreme experimental conditions of normal stress, acceleration, and sliding velocity. *J. Geophys. Res., Solid Earth* 116 (B7).
- Passelègue, F.X., Goldsby, D.L., Fabbri, O., 2014. The influence of ambient fault temperature on flash-heating phenomena. *Geophys. Res. Lett.* 41 (3), 828–835.
- Perrin, G., Rice, J.R., Zheng, G., 1995. Self-healing slip pulse on a frictional surface. *J. Mech. Phys. Solids* 43 (9), 1461–1495.
- Peyrat, S., Olsen, K., Madariaga, R., 2001. Dynamic modeling of the 1992 Landers earthquake. *J. Geophys. Res., Solid Earth* 106 (B11), 26467–26482.
- Platt, J.D., Brantut, N., Rice, J.R., 2015. Strain localization driven by thermal decomposition during seismic shear. *J. Geophys. Res., Solid Earth* 120 (6), 4405–4433.
- Platt, J.D., Rudnicki, J.W., Rice, J.R., 2014. Stability and localization of rapid shear in fluid-saturated fault gouge: 2. Localized zone width and strength evolution. *J. Geophys. Res., Solid Earth* 119 (5), 4334–4359.
- Proctor, B.P., Mitchell, T.M., Hirth, G., Goldsby, D., Zorzi, F., Platt, J.D., Di Toro, G., 2014. Dynamic weakening of serpentinite gouges and bare surfaces at seismic slip rates. *J. Geophys. Res., Solid Earth* 119 (11), 8107–8131.
- Reid, H.F., 1910. The mechanism of the earthquake. In: *The California Earthquake of April 18, 1906*. In: Report of the State Earthquake Investigation Commission, vol. 2. Carnegie Institution, Washington, DC, pp. 1–192.
- Rempe, M., Smith, S., Mitchell, T., Hirose, T., Di Toro, G., 2017. The effect of water on strain localization in calcite fault gouge sheared at seismic slip rates. *J. Struct. Geol.* 97, 104–117.
- Renner, J., Evans, B., Siddiqi, G., 2002. Dislocation creep of calcite. *J. Geophys. Res., Solid Earth* 107 (B12).
- Rice, J.R., 2006. Heating and weakening of faults during earthquake slip. *J. Geophys. Res., Solid Earth* 111 (B5).
- Rice, J.R., Rudnicki, J.W., Platt, J.D., 2014. Stability and localization of rapid shear in fluid-saturated fault gouge: 1. Linearized stability analysis. *J. Geophys. Res., Solid Earth* 119 (5), 4311–4333.
- Ruina, A., 1983. Slip instability and state variable friction laws. *J. Geophys. Res., Solid Earth* 88 (B12), 10359–10370.
- Rutter, E.H., 1972. The influence of interstitial water on the rheological behaviour of calcite rocks. *Tectonophysics* 14 (1), 13–33.
- Rutter, E.H., 1974. The influence of temperature, strain rate and interstitial water in the experimental deformation of calcite rocks. *Tectonophysics* 22 (3–4), 311–334.
- Segall, P., Rice, J.R., 2006. Does shear heating of pore fluid contribute to earthquake nucleation? *J. Geophys. Res., Solid Earth* 111 (B9).
- Schmid, S.M., Panozzo, R., Bauer, S., 1987. Simple shear experiments on calcite rocks: rheology and microfabric. *J. Struct. Geol.* 9 (5–6), 747–778.
- Schmid, S.M., Paterson, M.S., Boland, J.N., 1980. High temperature flow and dynamic recrystallization in Carrara marble. *Tectonophysics* 65 (3–4), 245–280.
- Sibson, R.H., Moore, J.M.M., Rankin, A.H., 1975. Seismic pumping—a hydrothermal fluid transport mechanism. *J. Geol. Soc.* 131 (6), 653–659.
- Smith, S.A.F., Nielsen, S., Di Toro, G., 2015. Strain localization and the onset of dynamic weakening in calcite fault gouge. *Earth Planet. Sci. Lett.* 413, 25–36.
- Stein, S., Wyssession, M., 2009. *An Introduction to Seismology, Earthquakes, and Earth Structure*. John Wiley & Sons.
- Sone, H., Shimamoto, T., 2009. Frictional resistance of faults during accelerating and decelerating earthquake slip. *Nat. Geosci.* 2 (10), 705.
- Spagnuolo, E., Plümper, O., Violay, M., Cavallo, A., Di Toro, G., 2015. Fast-moving dislocations trigger flash weakening in carbonate-bearing faults during earthquakes. *Sci. Rep.* 5, 16112.
- Tinti, E., Fukuyama, E., Piatanesi, A., Cocco, M., 2005. A kinematic source-time function compatible with earthquake dynamics. *Bull. Seismol. Soc. Am.* 95 (4), 1211–1223.
- Tsutsumi, A., Shimamoto, T., 1997. High-velocity frictional properties of gabbro. *Geophys. Res. Lett.* 24 (6), 699–702.
- Verberne, B.A., Niemeijer, A.R., De Bresser, J.H., Spiers, C.J., 2015. Mechanical behavior and microstructure of simulated calcite fault gouge sheared at 20–600 °C: implications for natural faults in limestones. *J. Geophys. Res., Solid Earth* 120 (12), 8169–8196.
- Violay, M., Di Toro, G., Nielsen, S., Spagnuolo, E., Burg, J.P., 2015. Thermo-mechanical pressurization of experimental faults in cohesive rocks during seismic slip. *Earth Planet. Sci. Lett.* 429, 1–10.
- Violay, M., Di Toro, G., Gibert, B., Nielsen, S., Spagnuolo, E., Del Gaudio, P., et al., 2014a. Effect of glass on the frictional behavior of basalts at seismic slip rates. *Geophys. Res. Lett.* 41 (2), 348–355.
- Violay, M., Nielsen, S., Gibert, B., Spagnuolo, E., Cavallo, A., Azais, P., et al., 2014b. Effect of water on the frictional behavior of cohesive rocks during earthquakes. *Geology* 42 (1), 27–30.
- Violay, M., Nielsen, S., Spagnuolo, E., Cinti, D., Di Toro, G., Di Stefano, G., 2013. Pore fluid in experimental calcite-bearing faults: abrupt weakening and geochemical signature of co-seismic processes. *Earth Planet. Sci. Lett.* 361, 74–84.
- Walker, A.N., Rutter, E.H., Brodie, K.H., 1990. Experimental study of grain-size sensitive flow of synthetic, hot-pressed calcite rocks. *Geol. Soc. (Lond.) Spec. Publ.* 54 (1), 259–284.
- Zoback, M.D., Harjes, H.P., 1997. Injection-induced earthquakes and crustal stress at 9 km depth at the KTB deep drilling site, Germany. *J. Geophys. Res., Solid Earth* 102 (B8), 18477–18491.
- Zheng, G., Rice, J.R., 1998. Conditions under which velocity-weakening friction allows a self-healing versus a cracklike mode of rupture. *Bull. Seismol. Soc. Am.* 88 (6), 1466–1483.